POLAR TIDE/PSI
start time: 04/23/03 04:19:58 UT
stop time: 04/23/03 04:49:59 UT
10 spins averaged
collapse option 2
spin marker at sun pulse

Stops

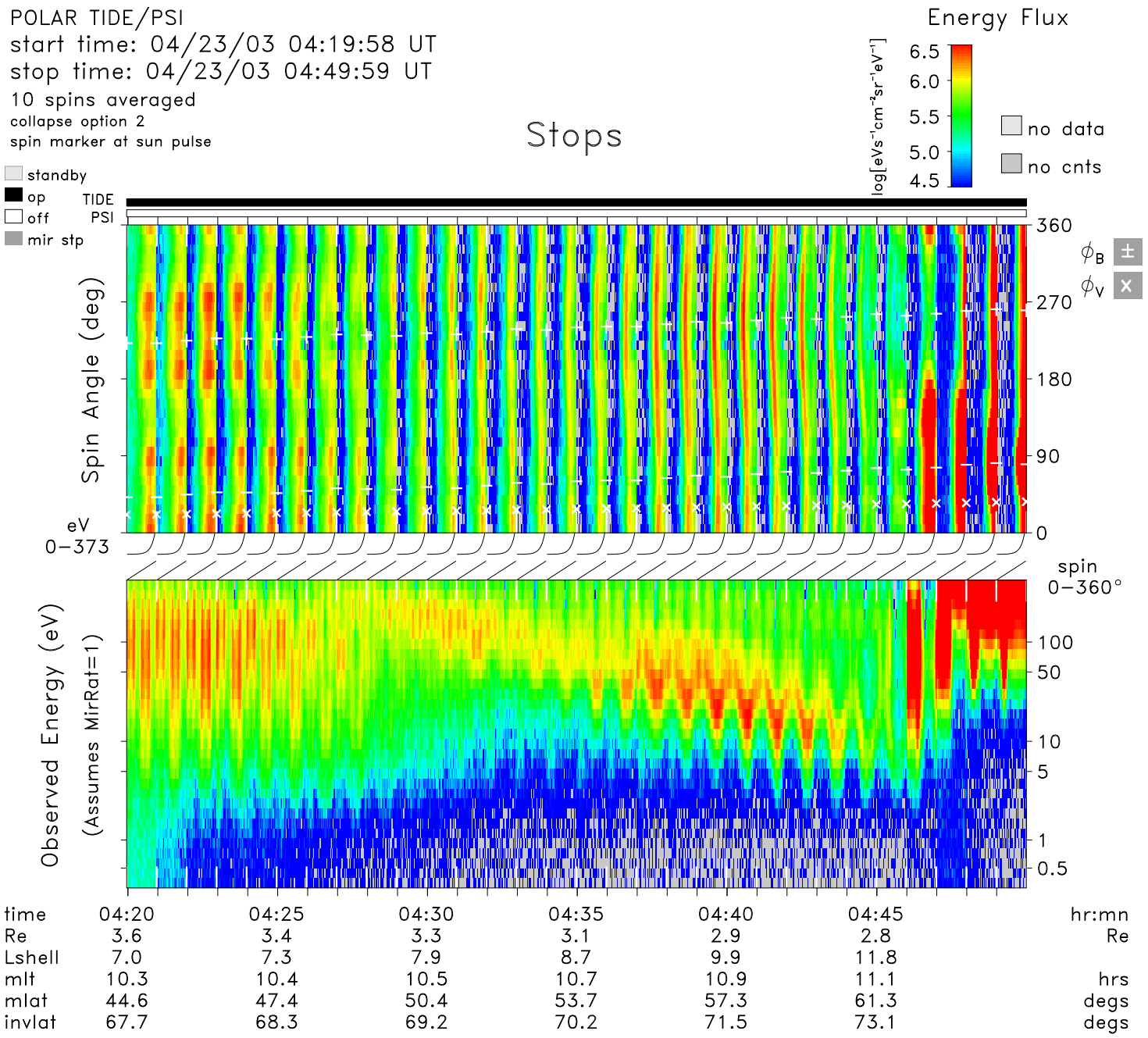

time	04:20	04:25	04:30	04:35	04:40	04:45	hr:mn
Re	3.6	3.4	3.3	3.1	2.9	2.8	Re
Lshell	7.0	7.3	7.9	8.7	9.9	11.8	
mlt	10.3	10.4	10.5	10.7	10.9	11.1	hrs
mlat	44.6	47.4	50.4	53.7	57.3	61.3	degs
invlat	67.7	68.3	69.2	70.2	71.5	73.1	degs

tide_lz_v5.5.1
Fri Apr 25 09:22:23 2003
plot: t0304230419_0449_sp.q20330.esse.ps
no minimum subtracted

sector_sens: no correction
calibration: tide_calib.v6
mass_calibration: mass_calib.v7
ion_mask: t030422_v2.mask

s/c potential = 0.0000
attitude: 03042302.cdf
orbit: 03042302.cdf
level-zero: 03042301.dat

POLAR TIDE/PSI
start time: 04/23/03 04:39:59 UT
stop time: 04/23/03 04:49:59 UT
4 spins averaged
collapse option 2
spin marker at sun pulse

Stops

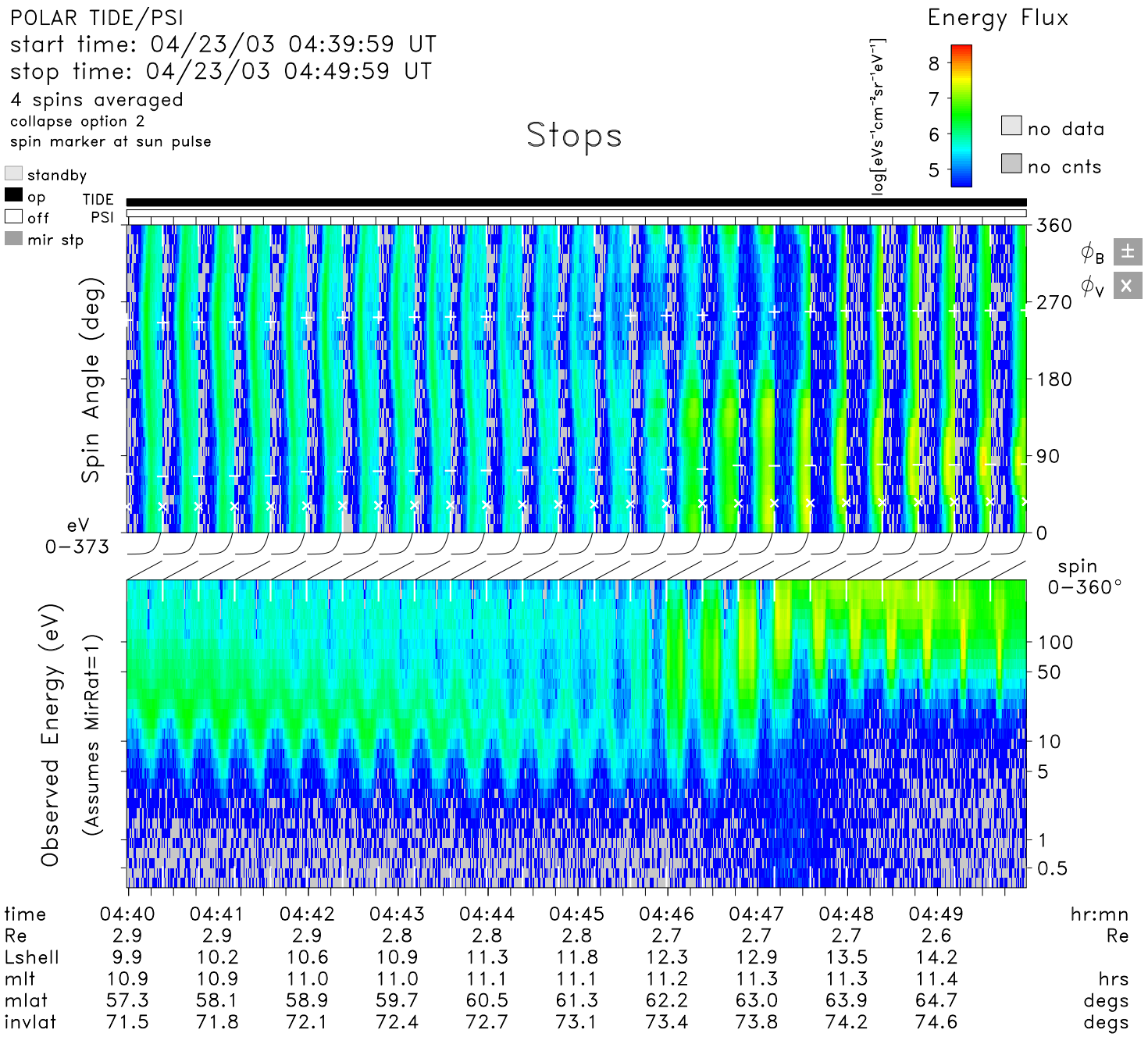

time	04:40	04:41	04:42	04:43	04:44	04:45	04:46	04:47	04:48	04:49	hr:mn
Re	2.9	2.9	2.9	2.8	2.8	2.8	2.7	2.7	2.7	2.6	Re
Lshell	9.9	10.2	10.6	10.9	11.3	11.8	12.3	12.9	13.5	14.2	
mlt	10.9	10.9	11.0	11.0	11.1	11.1	11.2	11.3	11.3	11.4	hrs
mlat	57.3	58.1	58.9	59.7	60.5	61.3	62.2	63.0	63.9	64.7	degs
invlat	71.5	71.8	72.1	72.4	72.7	73.1	73.4	73.8	74.2	74.6	degs

tide_lz_v5.5.1
Fri Apr 25 09:31:02 2003
plot: t0304230439_0449_sp.q20509.esse.ps
no minimum subtracted

sector_sens: no correction
calibration: tide_calib.v6
mass_calibration: mass_calib.v7
ion_mask: t030422_v2.mask

s/c potential = 0.0000
attitude: 03042302.cdf
orbit: 03042302.cdf
level–zero: 03042301.dat

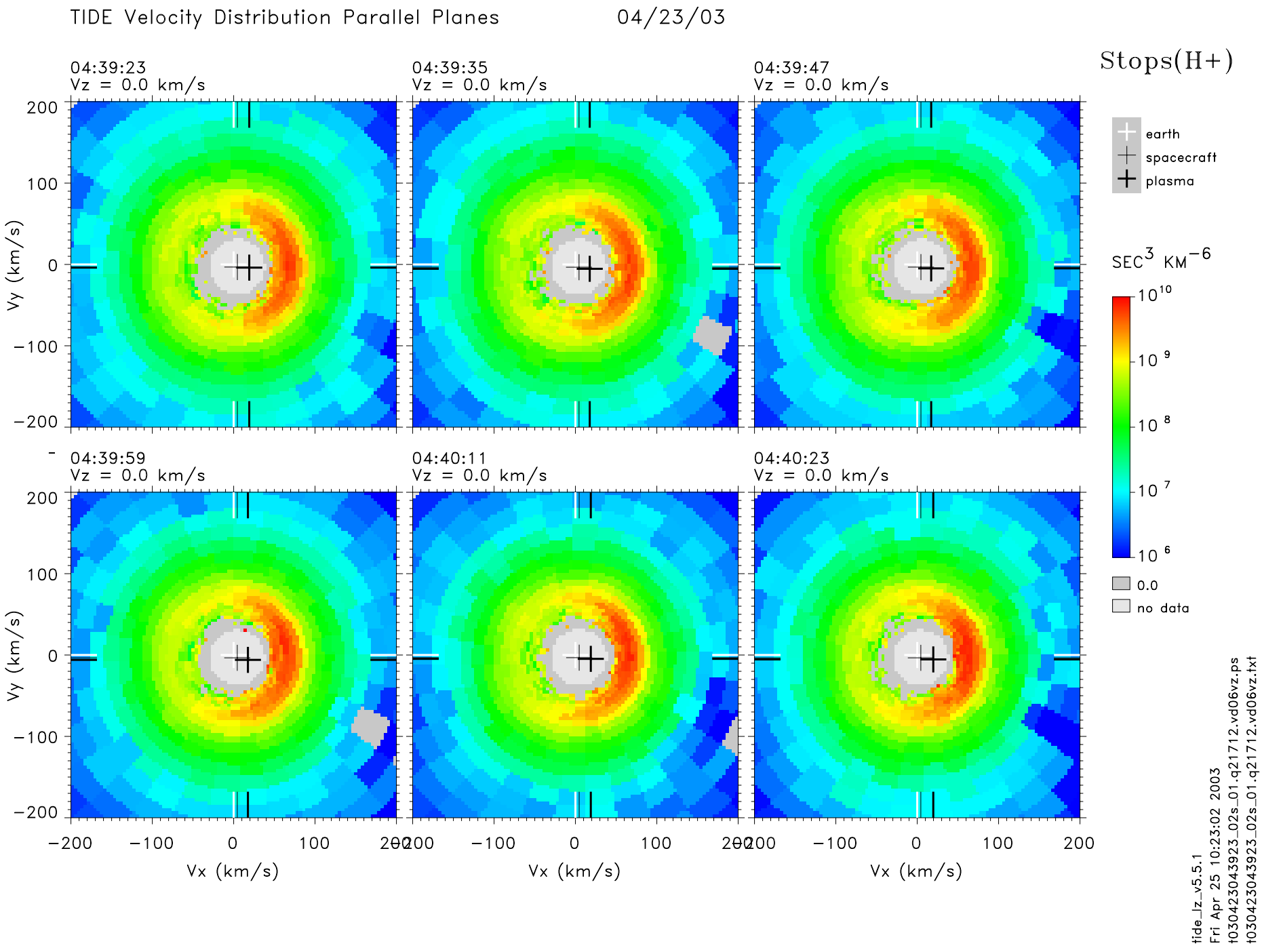
TIDE Velocity Distribution Parallel Planes
04/23/03
Stops(H+)
04:39:23
Vz = 0.0 km/s
04:39:35
Vz = 0.0 km/s
04:39:47
Vz = 0.0 km/s
04:39:59
Vz = 0.0 km/s
04:40:11
Vz = 0.0 km/s
04:40:23
Vz = 0.0 km/s
Vy (km/s)
Vx (km/s)
200
100
0
−100
−200
earth
spacecraft
plasma
SEC3 KM−6
10 10
10 9
10 8
10 7
10 6
0.0
no data
tide_lz_v5.5.1
Fri Apr 25 10:23:02 2003
t030423043923_02s_01.q21712.vd06vz.ps
t030423043923_02s_01.q21712.vd06vz.txt

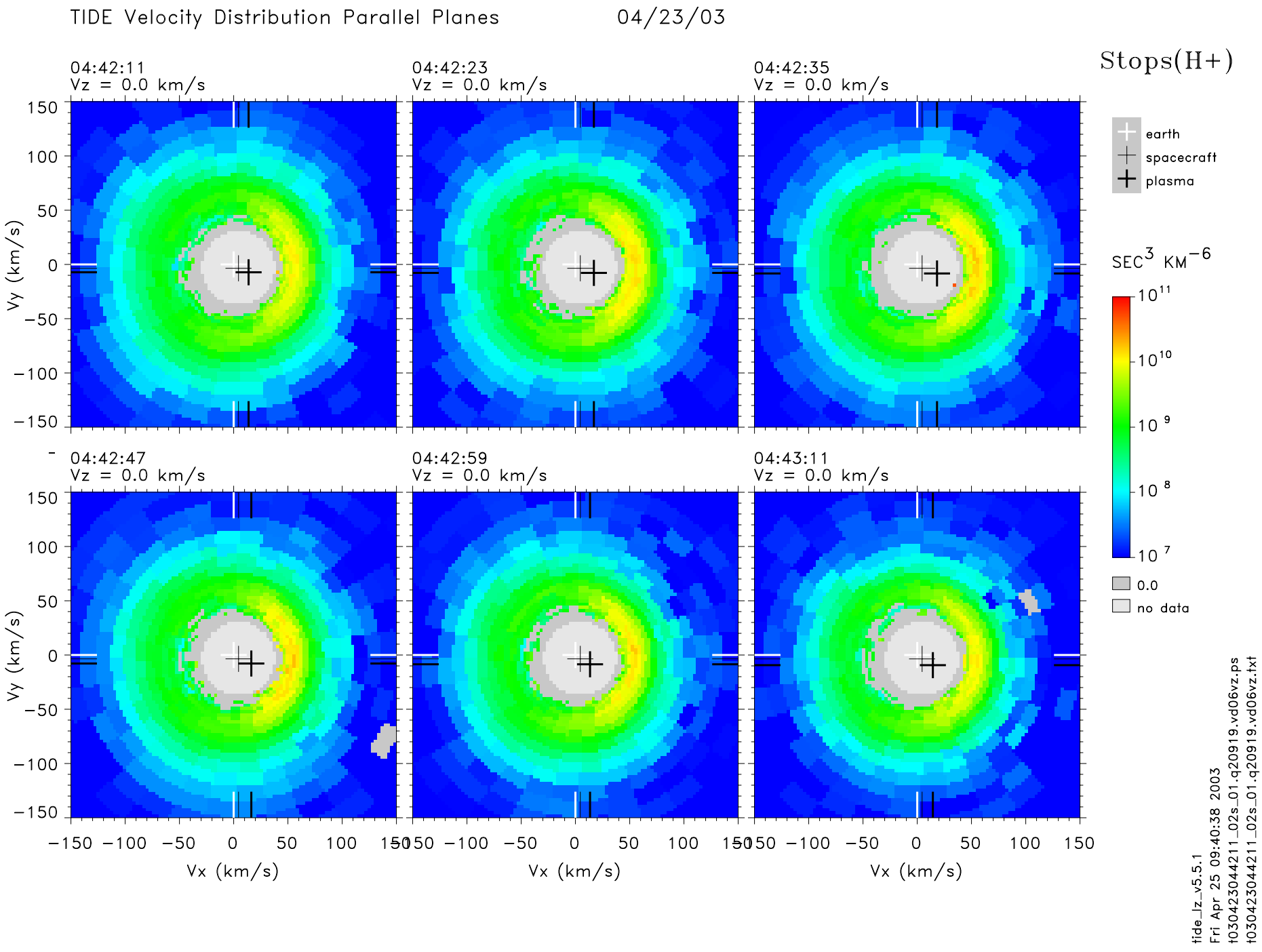
TIDE Velocity Distribution Parallel Planes
04/23/03
Stops(H+)
04:42:11
Vz = 0.0 km/s
04:42:23
Vz = 0.0 km/s
04:42:35
Vz = 0.0 km/s
04:42:47
Vz = 0.0 km/s
04:42:59
Vz = 0.0 km/s
04:43:11
Vz = 0.0 km/s
earth
spacecraft
plasma
SEC3 KM−6
10 11
10 10
10 9
10 8
10 7
0.0
no data
Vy (km/s)
Vx (km/s)
150
100
50
0
−50
−100
−150
tide_lz_v5.5.1
Fri Apr 25 09:40:38 2003
t030423044211_02s_01.q20919.vd06vz.ps
t030423044211_02s_01.q20919.vd06vz.txt

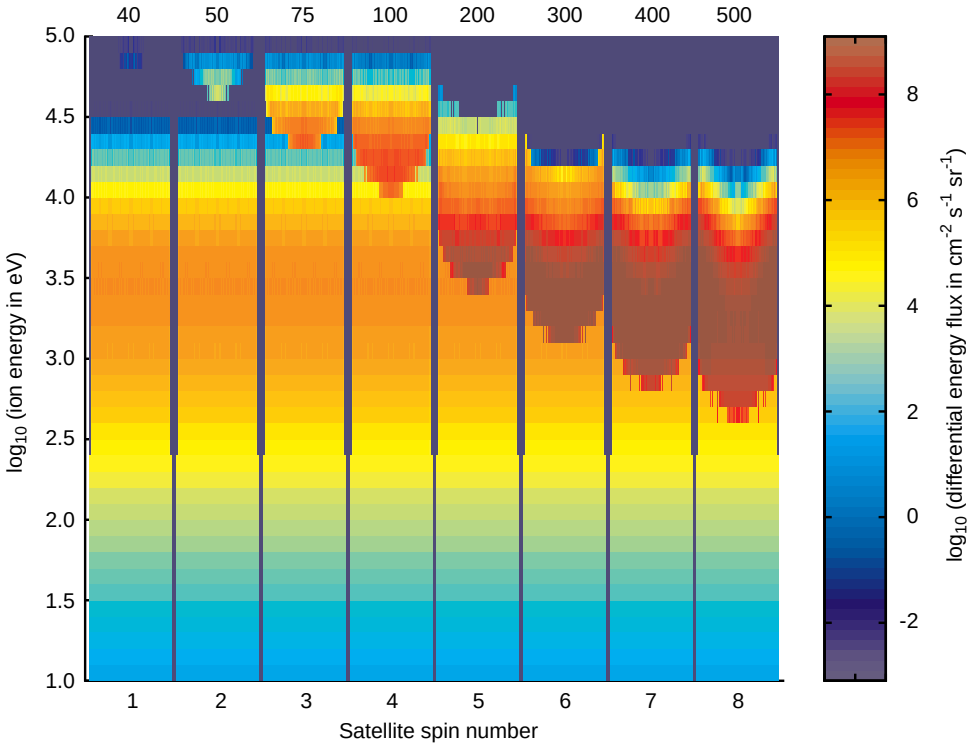

Fig. 7. Pitch-angle/energy spectra obtained by spins of a mid-altitude satellite at eight elapsed times since reconnection ($t_s - t_o$), as given at the top of each case. The differential energy flux is colour contoured (on a log scale) as a function of pitch angle and the logarithm of energy: in each panel, the pitch angle a_s varies from 180° to 0 (downward) and back to 180°.

development of the form from a bowl to a V was noted by Menietti and Burch (1988). Note that at the lower edge of the ion Vs, all ions have come from the reconnection site because they have the lowest energy and thus longest flight time T at that pitch angle a_s. As a result, this edge is not dependent on the contour level, but this is certainly not true of the upper edge of the V. Thus the width of the V (in energy at any one pitch angle) depends on the sensitivity of the instrument, specifically the geometric factor and the one-count level. As a result, the extent of the source region inferred from the V will depend on the instrument. This point is addressed further in the next section.

Comparison of Fig. 7 with observations shows that the model reproduces well the observed ion Vs in this spectrogram format. For example, Fig. 7 can be compared with the second panel of Fig. 2 of Kremser et al. (1995). In making this comparison, it must be remembered that Fig. 7 has not been convolved with any instrument response characteristics and many of the features shown will be below the one-count level. In particular, note that the J_E scale in Fig. 7 covers 12 decades, whereas the data presentation given by Kremser *et al.* (1995) covers only 3.7. For this reason, the low-flux features at the highest energies are not as clear in the data as they are in this model. Nevertheless, the data clearly reveal ions at higher energies than are seen equatorwards of the cusp on closed field lines. The bottom panel of Fig. 2 of Kremser *et al*: (1995) is from a high-energy-ion instrument which detects ions of energy up to about 100 keV, as in Fig. 7. These high-energy ions are observed to share the same energy/time-of-observation dispersion ramp as the cusp ions, as is also predicted in Fig. 7. Furthermore, from the ratios of the fluxes of different species, Kremser *et al.* (1995) find that these higher-energy ions are of magnetospheric origin and suggest that they are generated by interaction with the magnetopause. This is confirmed to be the mechanism in the modelling presented here.

Looking closely at the spin-angle distribution for $(t_s - t_o) = 500$ s, it can be seen that a minimum is starting to form at zero pitch angle, with peaks at larger values. This is also seen in the data presented by Kremser *et al.* (1995) and represents the evolution towards upgoing, mirrored mantle ions, as discussed by Rosenbauer et al. (1975).

Note that in Fig. 4, 5 and 7, the magnetospheric CPS ions (sp) are always seen at energies below the time-of-flight cut-off energy (which is defined by $T = t_s - t_o$ and so depends on the pitch angle and the time elapsed since reconnection), whereas the injected sheath ions and energised magnetospheric ions are simultaneously present above this cut-off energy. This predicted continuation of sp ions at energies below the injected magnetosheath ions is a feature of all observations of dispersed LLBL and cusp ions, at both middle and low altitudes.

4 Injection locations of observed cusp and LLBL ions

It is instructive to return to the debate about where the precipitating ions seen in the cusp region were injected across the magnetopause. As was discussed in the introduction, Menietti and Burch (1988) used the ion Vs modelled in Fig. 7 to derive a spread of source locations of about 1 R_E, whereas Lockwood and Smith (1993) argued that the spread of ion energies seen in low-

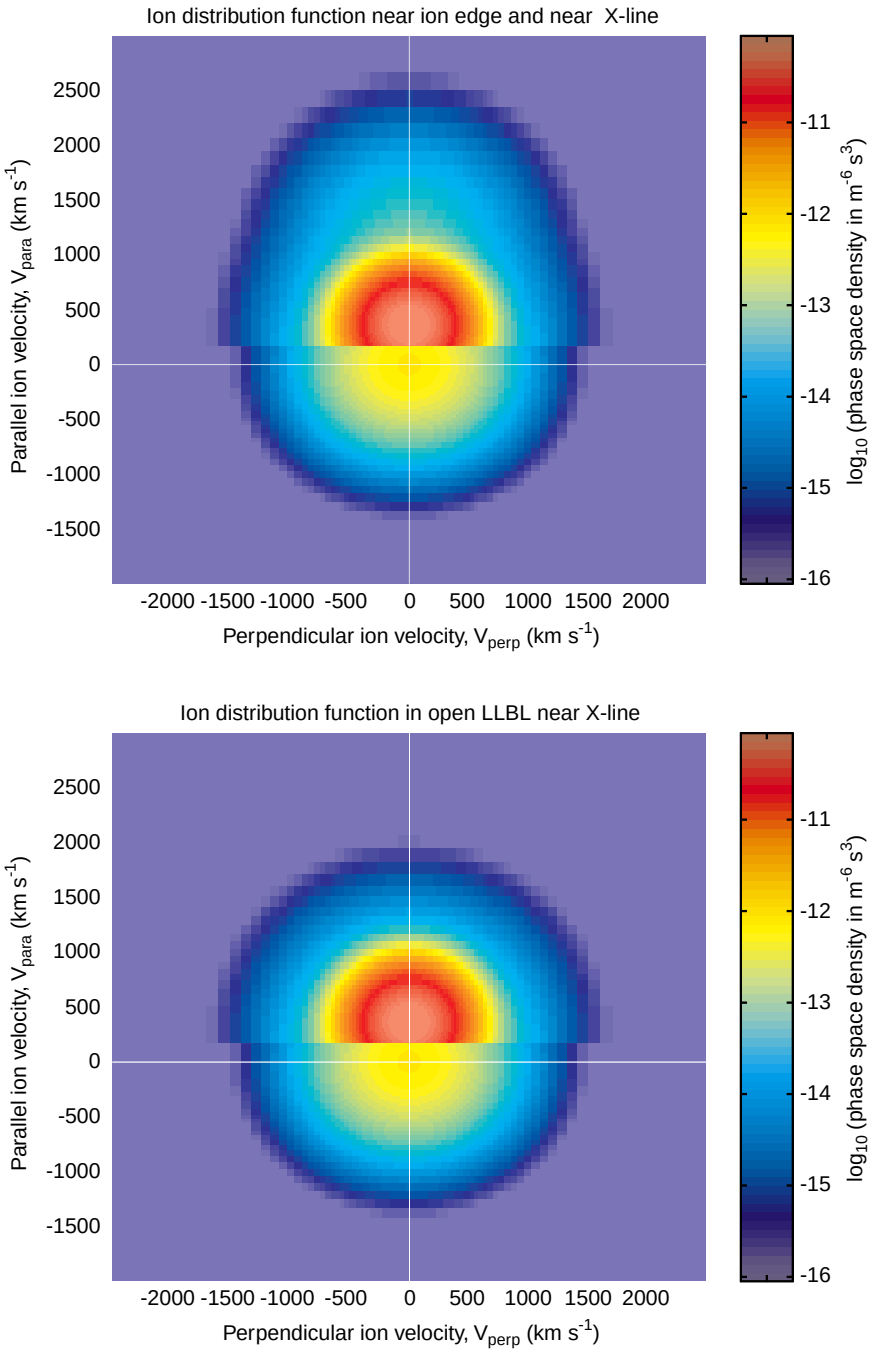

Fig. 2. Ion distribution functions in the open LLBL in the immediate vicinity of the reconnection X-line ($d_n \approx 0$, $t_n \approx 0$). The parallel velocity is positive towards the Earth and is in the Earth's frame of reference: (*top*) between the interior wave (i in Fig. 1) and the ion edge which is closer to the separatrix s; (*bottom*) between the exterior and interior waves (e and i)

the field line tailward and the time of flight of the ions from the magnetopause to the satellite.

In Fig. 4b, $(t_s - t_o) = 75$ s and two ion populations can be seen. The lower-energy population is a loss-cone distribution of the sp ions (i.e. CPS) which were present on closed field lines ($(t_s - t_o < 0)$ and have yet to be influenced by the fact that the field line has been opened. Note that it has been assumed here that equatorial scattering has filled the loss cone corresponding to mirror points in the opposite hemisphere; however, this assumption was not necessary and a double loss cone distribution could equally well have been used. At the satellite, the loss of sp ions is first noted at the highest energies as the lowest flight time sp ions fail to arrive: for $(t_s - t_o)$ as low as 75 s, only loss of ions with $T < (t_s - t_o) = 75$ s could be noted and the fluxes of such ions in the sp population is negligibly small. The boundary in $(V_\perp, V_\parallel)$ phase space defined by $T = (t_s - t_o)$ is here called the *time-of-flight cut-off*. Below this cut-off only the sp ions from the closed field-line region can be seen, above it only the populations generated by the open magnetopause (t-sh, re-sp and ri-sp) can be found. For reference with Fig. 3, the lower cut-off energy of field-aligned ions is given by:

$$E_{ic}(\alpha_s = O) = (m/2)\{s_x/(t_s - t_o)\}^2, \quad (5)$$

where s_x is the distance along the field line from the X-line to the altitude of the satellite, which is here 23.5 R_E.

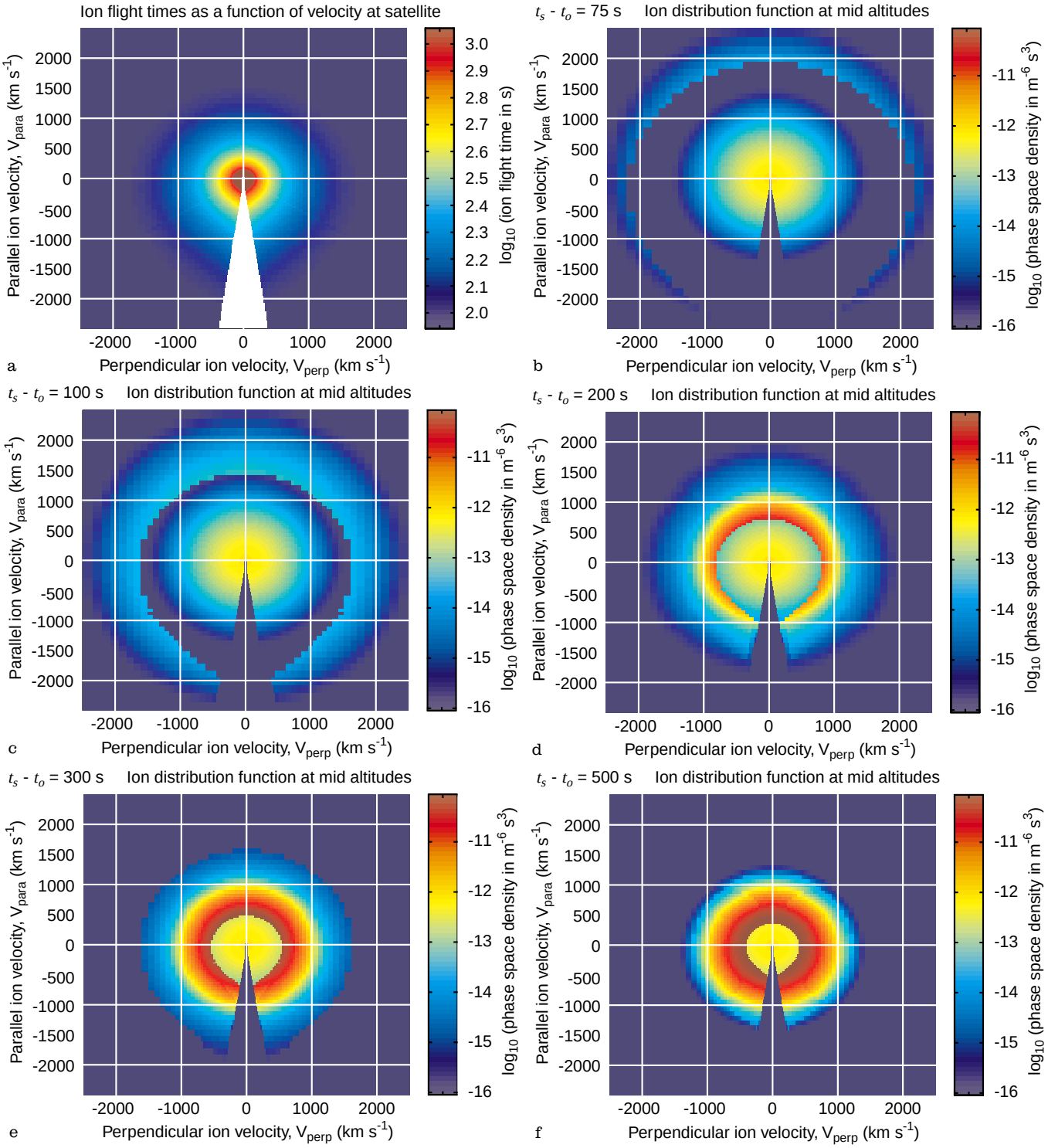

Fig. 4a. Ion flight time from a point P_n on the magnetopause to the altitude of satellite, T, colour coded (on a logarithmic scale) as a function of the field-parallel and field-perpendicular ion velocities at the satellite. In this example, P_n is at the (subsolar) reconnection site ($d_n = 0$, $t_n = 0$). **b–f** Ion distribution functions at the satellite; the elapsed time since reconnection ($t_s - t_o$) is: **b** 75 s; **c** 100 s; **d** 200 s; **e** 300 s; and **f** 500 s

cusp, for example as revealed by the sequence shown in Fig. 2 of Woch and Lundin (1992).

In cases such as that for $(t_s - t_o) = 200$ s, the magnetospheric (sp) ions below the cut-off appear to belong to the same population as those magnetospheric ions that have been reflected off the exterior wave (re-sp) and that are seen at energies above where transmitted sheath (t-sh) ions dominate: these two populations (sp and re-sp) could therefore be fitted with a single Maxwellian (of higher temperature and density than the sp population – cf. Fig. 3). This point is demonstrated in Fig. 6, in which the $J(E)$ spectrum for

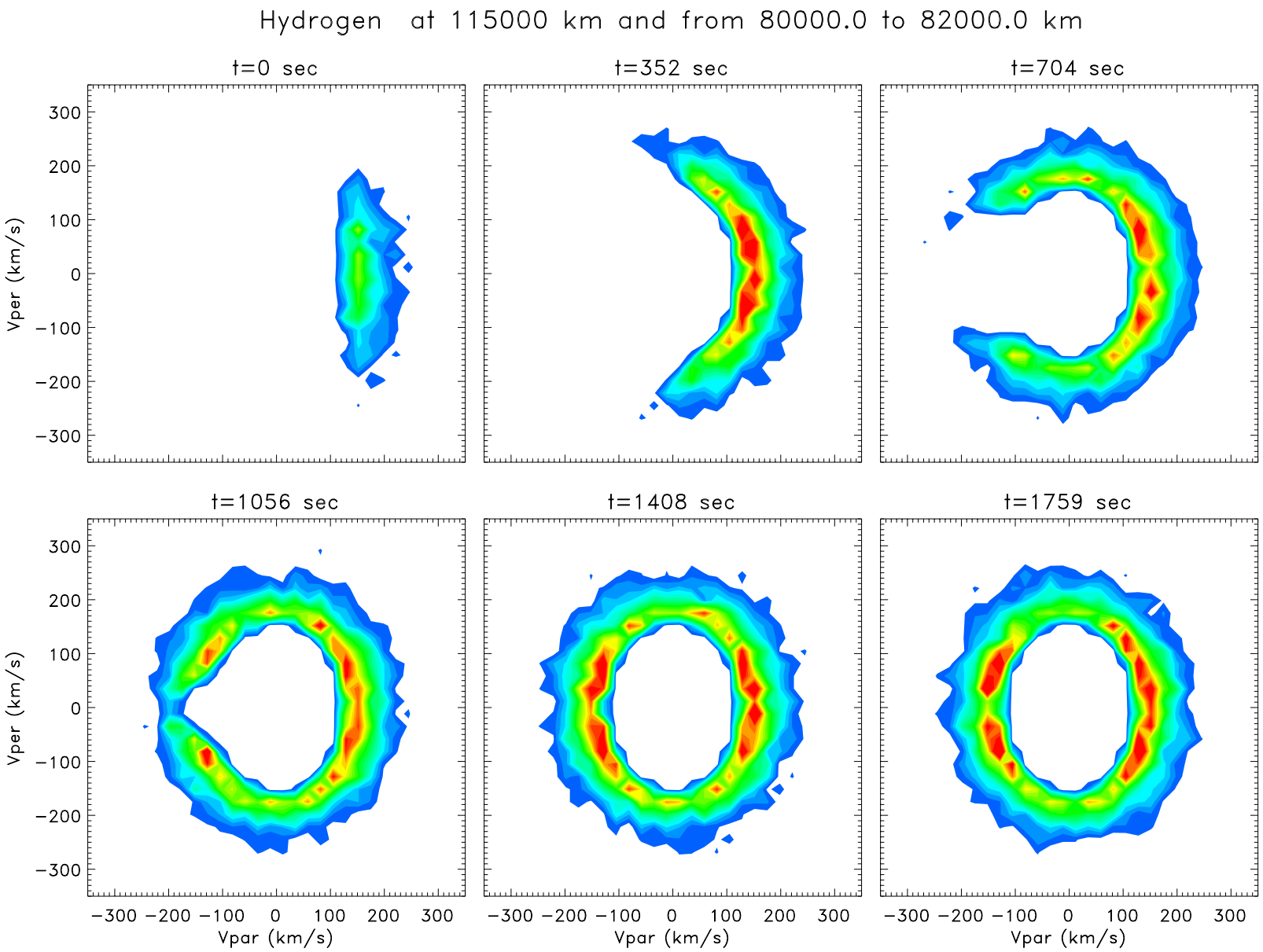

Thu May 29 13:41:09 2003